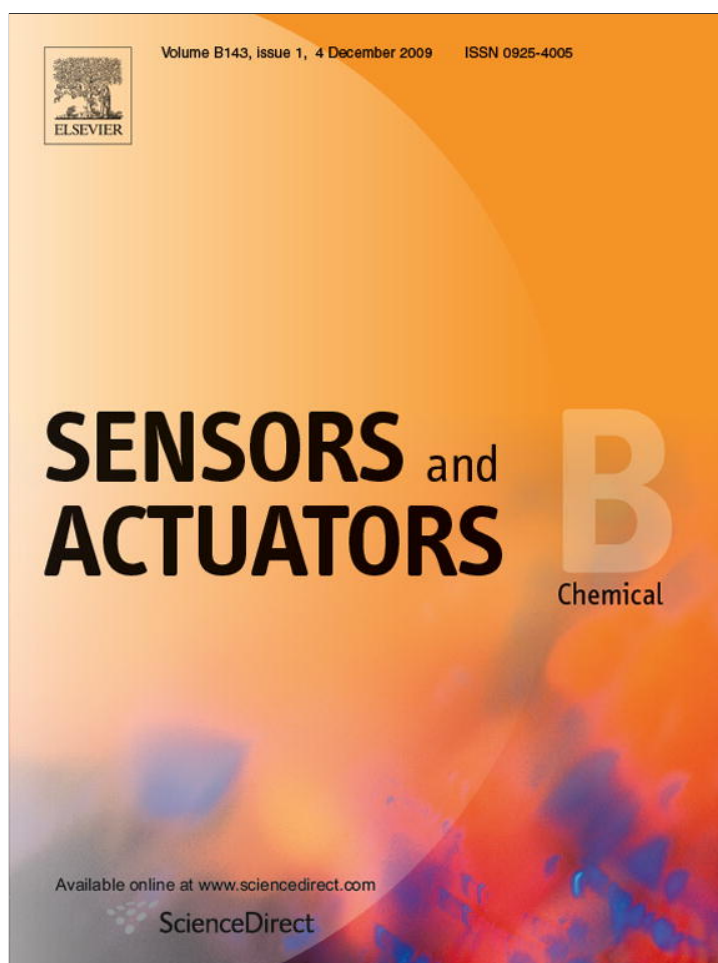


Provided for non-commercial research and education use.
Not for reproduction, distribution or commercial use.



This article appeared in a journal published by Elsevier. The attached copy is furnished to the author for internal non-commercial research and education use, including for instruction at the authors institution and sharing with colleagues.

Other uses, including reproduction and distribution, or selling or licensing copies, or posting to personal, institutional or third party websites are prohibited.

In most cases authors are permitted to post their version of the article (e.g. in Word or Tex form) to their personal website or institutional repository. Authors requiring further information regarding Elsevier's archiving and manuscript policies are encouraged to visit:

<http://www.elsevier.com/copyright>



Template-free synthesis and gas sensing properties of well-controlled porous tin oxide nanospheres

S.C. Yeow^a, W.L. Ong^a, A.S.W. Wong^b, G.W. Ho^{a,*}

^a Department of Electrical and Computer Engineering, National University of Singapore, 4 Engineering Drive, Singapore 117576, Singapore

^b Institute of Materials Research and Engineering, A*STAR (Agency for Science Technology and Research), 3 Research Link, Singapore 117602, Singapore

ARTICLE INFO

Article history:

Received 3 June 2009

Received in revised form 25 July 2009

Accepted 26 August 2009

Available online 3 September 2009

Keywords:

Tin oxide

Nanospheres

Hydrothermal

Mesoporous

Nanocrystalline

Sensor

Hydrogen

ABSTRACT

High yield of tin dioxide (SnO₂) nanospheres with various degrees porosity have been successfully synthesized without any physical template via an economical, easily scalable hydrothermal process. The porosity or the specific surface area of SnO₂ nanospheres can effectively be tuned via precursor concentration, temperature and the removal of additive urea. Higher reaction temperature, low precursor concentration and elimination of urea additive favorably increase the porosity of the nanospheres. The gas sensing properties of the nanospheres show that the operating temperature has a strong influence on the response of the sensor whereby a higher operating temperature leads to greater change in conductance and hence, greater response. Other than the specific surface area, pore diameter of the nanospheres has shown to have an effect on the sensing behaviour. The response time is dependent on the operating temperature, 90% of resistance change ($R_{\text{air}}-R_{\text{gas}}$) was achieved within the first 1.3–3.0 min.

© 2009 Elsevier B.V. All rights reserved.

1. Introduction

There has always been a high demand for chemical sensors specially developed for environmental and medical monitoring and control. Metal oxides are widely used as gas sensing materials since they are high in sensitivity, reliability, inexpensive and relatively easy to be synthesized. As an n-type tin dioxide SnO₂ semiconductor has a wide band gap ($E_g = 3.6$ eV) with high chemical and thermal stability, it has attracted considerable research efforts in its applicability as gas sensors [1–3]. In addition, there has been a growing interest in the fabrication of hollow or porous inorganic nanostructures for gas sensors [4]. The large specific surface area of these porous nanostructures makes them very reactive materials since a high proportion of atoms are located at the surface of nanocrystals [5]. It was reported that hollow SnO₂ nanospheres exhibited enhanced room temperature gas sensitivity as compared to SnO₂ nanoparticles of the same size [6]. The superior sensing performance can be attributed to the higher surface area of hollow SnO₂ nanospheres which provides more sites for surface adsorption and desorption of the gas molecules.

Hollow or porous nanostructures have typically been synthesized with the assistance of hard templates like sacrificial polymeric

core supports [7], or soft templates like micelles [8]. However, the removal of hard templates require complex synthetic procedures and high costs which limit their use in large-scale productions [9], while soft templating routes suffer from instability problems which require the introduction of complex surfactant systems [10]. It is also noted that additive-free synthesis of nanostructures and self-assembling them into well-defined porous nanospheres remains a huge challenge. However herein, we report a successful facile self-assembly, template and additive-free synthesis of porous SnO₂ nanospheres via hydrothermal process. The SnO₂ nanospheres obtained possess tunable specific surface areas depending on the internal structural morphologies which can be effectively controlled via changes in reaction conditions such as precursor concentration, reaction temperature and urea additives. The SnO₂ nanospheres show various sensitivities with the change in the porosity of the nanospheres and the operating temperatures of the sensors. In addition, the response and recovery times are dependent on the operating temperature of the nanospheres sensors. The mesoporous structures have shown to provide an enhancement in the surface area and sensitivity within the active sensing area.

2. Experimental section

Mesoporous nanospheres were synthesized through a simple hydrothermal method using potassium stannate trihydrate (K₂SnO₃·3H₂O, Aldrich 99.9%) as a precursor in an

* Corresponding author. Tel.: +65 65168121; fax: +65 67754710.
E-mail address: elehgw@nus.edu.sg (G.W. Ho).

Table 1
Summary of the growth conditions and the specific surface area of the samples.

Samples	Temp. (°C)	Conc. (mM)	Additives	Specific SA (m ² /g)
Ref	150	5	Yes	101.4
S1	150	5	No	142.3
S2	150	20	No	72.5
S3	225	5	No	156.4

ethanol–deionized water mixed solvent [11]. In a typical experiment, 5 mmol (mM) of $K_2SnO_3 \cdot 3H_2O$ was dissolved in 30 ml of ethanol–deionized water mixture (equal volumes of ethanol and water). After stirring for 5 min, a homogeneous solution was obtained and 0.1 M of urea was added to the mixture before transferring to a 40 ml Teflon-lined stainless steel autoclave. The autoclave was maintained at 150 °C for 24 h and then cooled down naturally to room temperature. The resulting white precipitate was centrifuged and thoroughly washed with ethanol before drying in air at 40 °C. The parameters affecting the morphology and porosity of the synthesized SnO_2 nanostructures are investigated by varying various experimental conditions. The gas sensing measurements were carried out after the synthesis of the nanospheres. The sensor electrodes were fabricated using a conventional photolithography on SiO_2 substrate. The finger electrodes were thermally evaporated with 200 nm of Ti/Au. The nanospheres were dispersed in water and were drop-casted onto the Au electrodes. An electrometer system was connected and controlled via a computer, interface by the software LabView to measure the change conductance while cycling H_2 (500 ppm) and dry air. The response of a gas sensor can be defined quantitatively as the ratio of the electrical resistance in air (R_a) to that in a sample gas (R_g).

Scanning electron microscopy (SEM) observations were carried out on a FESEM JSM-6700F operating at 10 kV. Transmission electron microscopy (TEM) characterisations were conducted using a JEOL-2100 TEM with an accelerating voltage of 200 kV. X-ray diffraction (XRD) experiments were performed on a Bruker GADDS XRD using monochromatized $Cu K\alpha$ ($\lambda = 0.154$ nm) radiation under

40 kV and 40 mA. Brunauer Emmett Teller (BET) measurements were conducted using a BET surface area and pore analyzer Autosorb (NOVA 3000) with N_2 as the adsorbate at liquid nitrogen temperature.

3. Results and discussion

We have systematically investigated various reaction parameters as shown in Table 1 to tune the morphology and porosity of the SnO_2 nanospheres without the use of physical template. It was found that the reaction temperature, concentration of the precursor and the removal of additive, urea affect the hollowing out of the interior of the nanospheres which directly correlate to the specific surface area. The morphology of the SnO_2 nanostructures produced under reference condition is shown in Fig. 1a. The nanospheres are well-dispersed with diameters between 50 and 200 nm. For the case of the synthesis without urea, a low precursor concentration of 5 mM has shown to yield monodispersed nanospheres. Fig. 1b shows the morphology of nanospheres synthesized without the addition of urea additive where the nanospheres remain well-dispersed and retain their general geometry and morphology. As the precursor concentration is increased to 10–20 mM (without the use of urea), severe agglomeration set in as the nanospheres lose their spherical morphology and form irregular structures. With a drastic increased in the concentration of precursor (20 mM of $K_2SnO_3 \cdot 3H_2O$), highly agglomerated and wide distribution of 50–500 nm diameters of as-synthesized nanospheres are observed (Fig. 1c). Next, the effect of higher growth temperature of 225 °C was studied which yields nanospheres of diameter 30–120 nm with relatively rough surfaces (Fig. 1d).

The specific surface area of the nanospheres produced by different reaction conditions is measured using BET (Table 1). The nitrogen physisorption isotherm exhibits a steep increase in the volume of adsorbed nitrogen, typical of pore condensation in mesoporous materials with uniform pore sizes. In comparison, the specific surface area of sample reference with urea is relatively

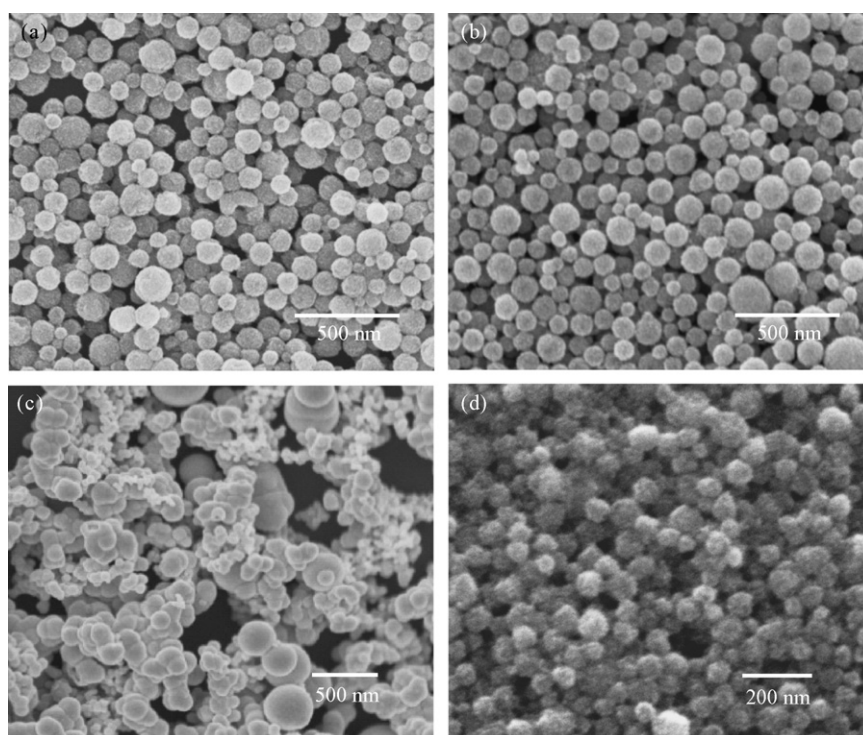


Fig. 1. SEM images of SnO_2 nanospheres synthesized at various reaction conditions (a) reference, (b) S1, (c) S2 and (d) S3.

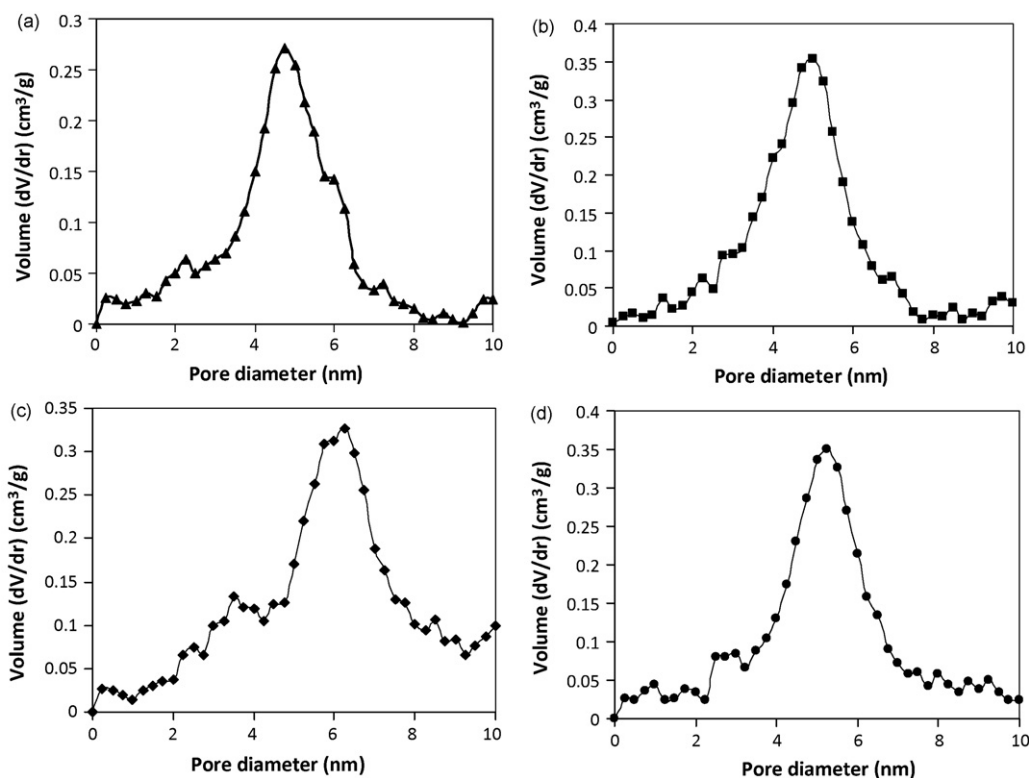


Fig. 2. The BJH pore diameter distribution plots of (a) reference, (b) S1, (c) S2 and (d) S3 samples, respectively.

lower ($101.4\text{ m}^2/\text{g}$) while sample S1 grown without urea at lower temperature (150°C) has a higher specific surface area ($142.3\text{ m}^2/\text{g}$). The sample S3 grown without urea and at higher temperature (225°C) exhibits the highest specific surface area of $156.4\text{ m}^2/\text{g}$. The lowest specific surface area ($72.5\text{ m}^2/\text{g}$) is measured from the sample S2 grown at high precursor concentration, as evidently, the produced nanospheres are highly agglomerated with possibly lower surface adsorption area. The BJH pore diameter distribution plots (Fig. 2) of reference, S1, S2 and S3 samples show peak at 4.8, 5.0, 6.3 and 5.3 nm, confirming a high degree of uniformity of the pores, respectively.

TEM imaging was carried out to access and analyze the internal structure of the as-synthesized nanospheres under various reaction conditions. Fig. 3a and b shows the nanospheres obtained at 5 mM precursor concentration at 150°C with and without addition of urea. TEM images show no significant change in morphology and porosity. In the case where there are overlapped of nanospheres dispersion (as indicated by arrows), the underlying nanospheres can be visibly observed, which suggest that the nanospheres are porous in nature. However, the nanospheres synthesized at higher precursor concentration (20 mM) show highly agglomerated structures with less porous structure (Fig. 3c and d). In some areas, the agglomerated structures are too thick to be electron transparent. The wide diameter distribution corroborated with the SEM results. Next, nanospheres grown at higher reaction temperature of 225°C are observed to be highly porous (Fig. 3e and f). High resolution image (Fig. 4a and b) reveals the nanospheres are made up of individual nanocrystallites of $\sim 5\text{--}10\text{ nm}$. The lattices fringes are measured to be 0.26 and 0.33 nm which can be indexed to the SnO_2 (1 0 1) and (1 1 0) crystal planes, respectively (Fig. 4b) [11]. From the TEM observations, it is evident that precursor concentration and reaction temperature affect the degree of porosity which in turn affects the specific surface area of the nanospheres.

The phase and purity of the sample were determined by XRD. Fig. 5 illustrates the typical diffraction pattern of the reference

and the samples synthesized without urea at 150°C . All the peaks can be well indexed to a tetragonal rutile SnO_2 structure (JCPDS card No. 41-1445, $a_0 = 4.738\text{ \AA}$, $c_0 = 3.187\text{ \AA}$). No characteristic peaks were observed for other impurities. It is important to note that the samples synthesized without urea does not compromise on the crystallinity quality or structural composition of the end-products. FTIR spectra of the nanospheres prepared with and without urea have been previously reported that urea molecules remains incorporated in the SnO_2 nanospheres [11]. The elimination of urea from the synthesis process removes any organic contaminant in the nanospheres. The elimination of additive brings the benefit of increasing the effective surface area as well as dismissing the need for subsequent high-temperature annealing to remove the adsorbed organic urea.

The possible formation mechanism of the mesoporous SnO_2 spheres has been postulated [11]. In the initial stage of the synthesis, the hydrolysis of potassium stannate trihydrate leads to the formation of numerous nanocrystallites, which have been observed by the TEM. These primary nanocrystallites are driven by the system surface energy reduction mechanism to aggregate. The formation of nanospheres by aggregation of nanocrystallites is closely referred to the imperfect oriented attachment mechanism [12]. This mechanism is based on self-assembly of primary nanocrystallites followed by spontaneous lattice fusion of the adjacent crystallographic planes in an ideal liquid environment medium. The nanocrystallites are randomly oriented but on a whole self-assembled to form porous spherical nanospheres.

Fig. 6a shows a typical sensor which has been fabricated with dispersed SnO_2 nanospheres. Current against voltage (I - V) measurements were obtained on the sensor by sweeping the applied voltage from -8 to 8 V . A typical stable current reading as shown in Fig. 6b clearly demonstrates that the SnO_2 nanosphere film provides a connecting Schottky electrical contact between pairs of Au electrodes. Fig. 6c shows the I - V measurements (ref, S1 and S3) in the range of -2 to 2 V . The variation in current is the highest for the

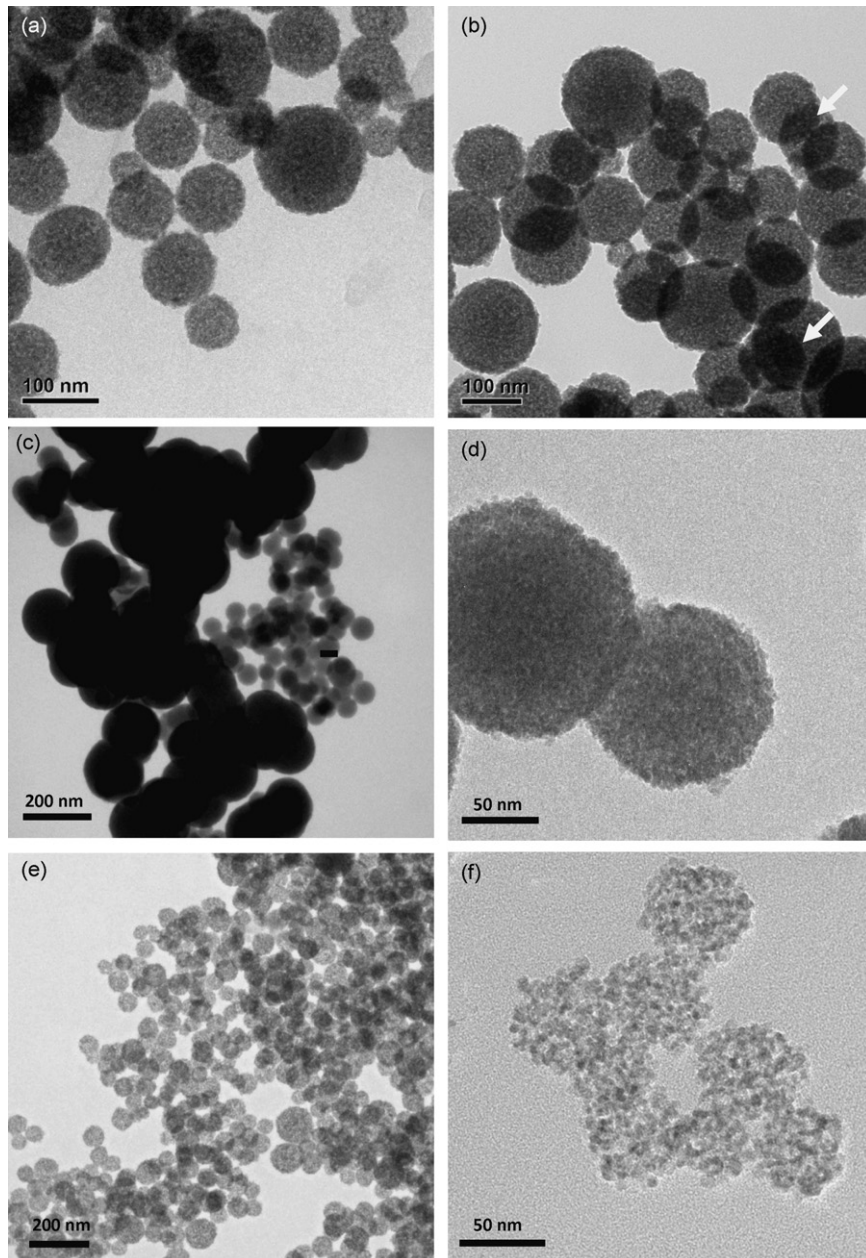


Fig. 3. TEM of SnO₂ nanospheres synthesized at various reaction conditions (a) reference, (b) S1 (c and d) S2 and (e and f) S3.

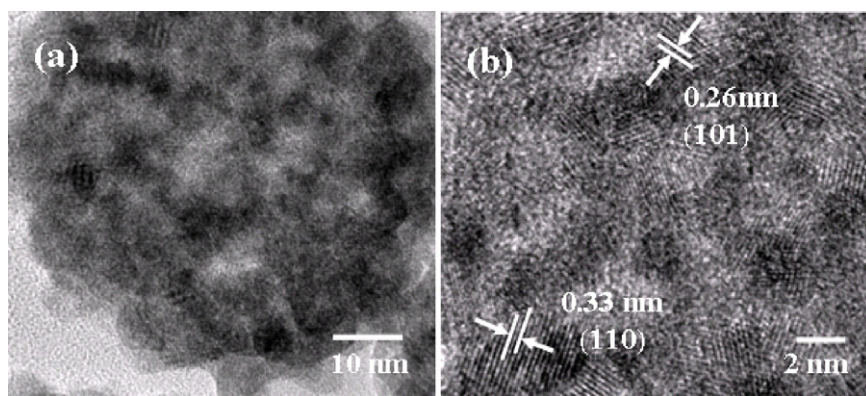


Fig. 4. (a) Low and (b) high resolution TEM images of SnO₂ nanospheres.

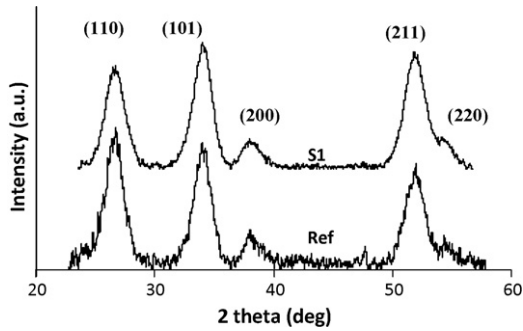


Fig. 5. XRD spectrum of the reference and S1 samples.

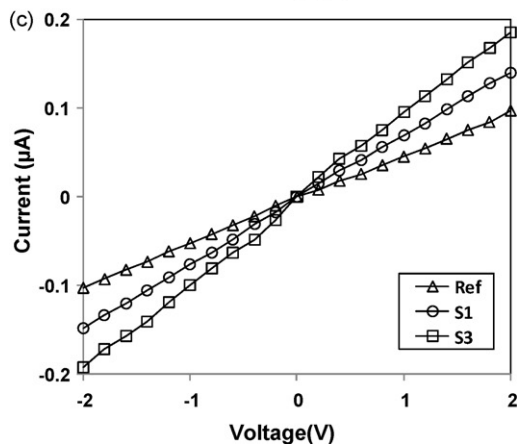
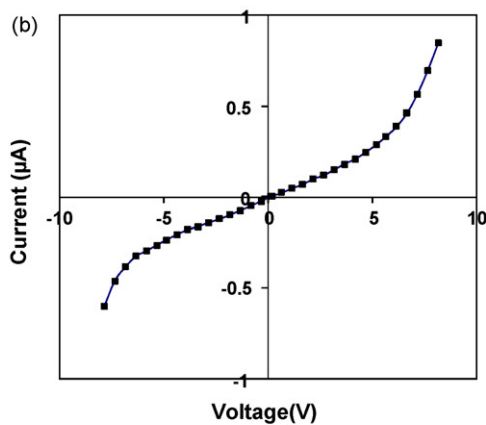
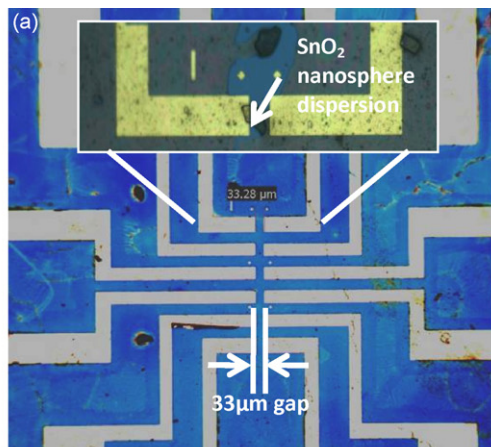


Fig. 6. (a) Optical image of the fabricated sensor and (b and c) room temperature I–V characteristics of the SnO₂ nanosphere sensors measured at different bias.

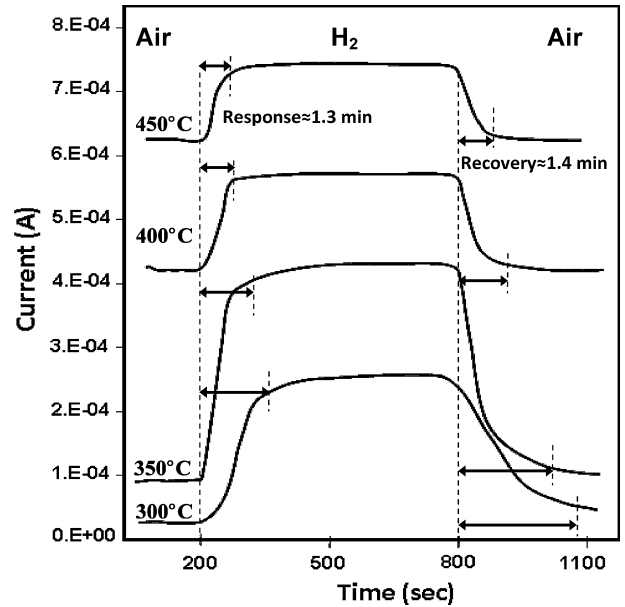
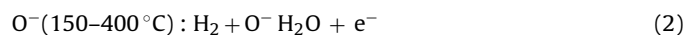
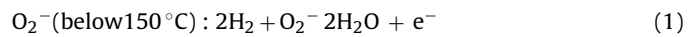


Fig. 7. Response and recovery times of the nanospheres sensor at various operating temperatures.

S3 sample and is in the range of 0.2 μA at 2.0V bias. The power consumption is 0.4 μW at this operating voltage. The reversible chemisorption of reactive gas, H₂ of the oxide nanospheres based sensor is then measured to produce a variation in conductance. Fig. 7 shows the current response graphs obtained from the reference sample by cycling it alternately in dry air and H₂ at various operating temperature. From the graphs, it is evident that when H₂ is introduced into the chamber, the current increases. This corresponds to a decrease in resistance of the material. The decrease in resistance is due to re-injection of electrons into the semiconductor when H₂ gas reacts with the adsorbed oxygen ions on the surface of the semiconductor. Similarly, when H₂ gas is removed from the chamber, the resistance increases and recovers to its original conductance. It is noted that the response time (90% of R_{air}–R_{gas}) is achieved within the first 1.3–3.0 min while the recovery time is 1.4–4.6 min, depending on the operating temperature of the sensor. The response time decreases from 3.0, 2.1, 1.4 to 1.3 min, as the operating temperature increases from 300 to 450 °C. This is due to the higher reaction rate of H₂ gas species on the surface of the nanospheres. The response and recovery times have been linked to the diffusion rate of the analyte gas into the sensing material, which in turn depends on the porosity and thickness of active film [13]. An active sensing material with large mean pore size allows all percolation paths in the sensing layer to be easily accessed by the analyte molecules, thereby leading to shorter response and recovery times.

The effect of operating temperature of the reference sample on the sensor performance is investigated. The responses of the sensor at different operating temperatures (200–450 °C) are shown in Fig. 8a. The operating temperature has a strong influence on the response of the sensor since the adsorption and desorption of oxygen ions on the surface of the semiconductor material is affected by the surrounding temperature. At low temperatures below 150 °C, oxygen is adsorbed on the surface predominantly as O₂[–] ions and as O[–] ions between 150 and 400 °C [13].



From the two Eqs. (1) and (2) presented above, it can be observed that for O₂[–], two molecules of H₂ are required to re-inject one electron into the semiconductor. This is twice the condition required for

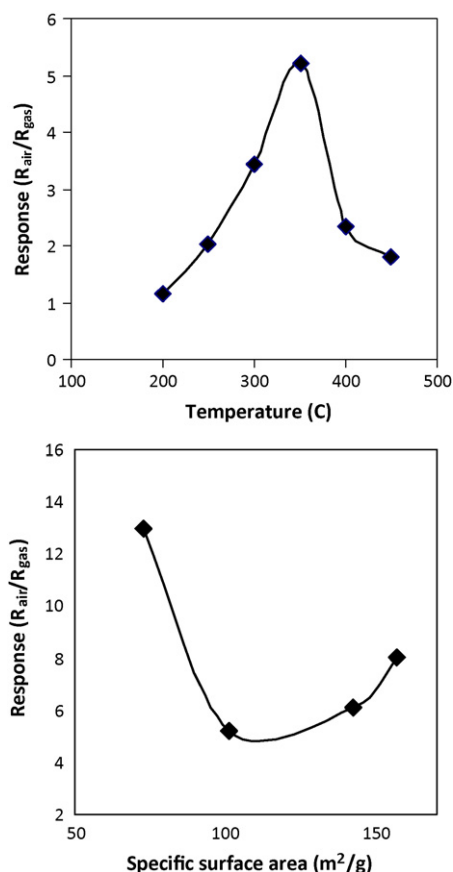


Fig. 8. Response plot versus (a) operating temperature and (b) specific surface area of SnO_2 nanospheres sensors.

the case of O^- which is formed at higher temperatures. As such, a higher operating temperature leads to a greater change in conductance and hence, greater response. On the other hand, desorption of all oxygen ionic species previously adsorbed occurs at high temperatures which explains the reduction in response as operating temperature is increased beyond the optimum value [14].

Next, the effect of specific surface area on the gas sensing performance is studied. Fig. 8b shows the response plot obtained at $350^\circ C$ for all the samples with different specific surface areas as reflected in the Table 1. It can be observed that the response increases with specific surface area for the reference, S1 and S3 samples. As discussed earlier, the gas sensing mechanism of the SnO_2 sensor depends on the surface reaction of oxygen species adsorbed on the semiconductor surface with H_2 . Hence, an increase in specific surface area of the sensor implies that there are more surface sites for oxygen adsorption which leads to greater surface reactivity with H_2 . This in turn causes a larger change in conductance and therefore, greater response. The correlation between surface area of sensor and sensitivity has been widely reported in earlier studies [15,16]. Additionally, some researchers have suggested that sensitivity increases linearly with surface area [14]. However, in our case the straightforward linear relationship between response and surface area is not observed for all samples. S2 sample has a lowest specific surface area of $72.5 m^2/g$, yet the response is noticeably the highest. These observations suggest that the response of the sensor is also dependent on other factors and not solely surface area. Shimizu et al. have prepared mesoporous SnO_2 structures with very high specific surface areas but also found slight differences in H_2 response among the sensors, irrespective of a large change in specific surface area of sensor materials [17,18]. A possible explanation offered is that the inner surfaces of the porous nanospheres are

not fully utilized for gas detection due to the limitation of diffusion of the analyte gas [17,18]. Other than the specific surface area, porosity of the sensing material can have an effect on the sensing behavior [17]. In mesopores structure, the mean free path of gas analyte molecules is determined by the characteristics of the pores of the sensing material [19]. If we assume that the gas diffusion follows a Knudsen flow, then the diffusion coefficient D_k is proportional to the pore radius, r as defined by the Eq. (3) in which R is the universal gas constant and M is the molecular weight of the gas molecule [17].

$$D_k = \frac{4r}{3} \sqrt{\frac{2RT}{\pi M}} \quad (3)$$

From Eq. (3), it is known that the pores have to be sufficiently wide for efficient diffusion of the gas molecules, resulting in higher sensitivity. The benefit of a high specific surface area must not be thwarted by limitations in the accessibility of surface of the sensing material.

It can be derived from the studies of the porosity of the SnO_2 nanospheres (Fig. 2) that the pore size of the reference, S1 and S3 are between 4.8 and 5.3 nm while S2 has the largest pore size of 6.3. It has been known that smaller pore size has higher specific surface area, but lower diffusion coefficient [19]. Gas diffusion is generally slower in smaller pores which can possibly explain the fact that the inner surfaces of the reference, S1 and S3 porous nanospheres are not fully utilized for gas detection due to the limitation of diffusion of the analyte gas. Hence, the sensing properties of nanospheres sensors are influenced not only by gas reactivity on the surface, but also highly dependent on gas diffusivity through the sensing layers, which might explain the modest increase in sensitivity with respect to the surface area obtained in the present study. As for the sample S2 which has the largest pore size which means less compact pore network, it does not limit the gas diffusion into the internal surfaces of the nanospheres. In addition, to the larger intraparticle pore size, the interstices between adjacent nanospheres (interparticle) are larger as well (due to the larger and non-uniformity of the nanospheres' diameter), which may allow both the exterior and interior of the nanospheres to be fully accessible to gas diffusion, which further increase the available active surface area. This in turn translates into higher gas sensitivity. The exact morphological and electrical aspects responsible for various sensing characteristics of the nanospheres are not exactly clear at the present moment. More studies to examine the structural parameters such as diameter of the nanospheres, pore size, pore distribution, etc. can be carried out to better understand the sensing properties of the porous nanospheres.

4. Conclusion

The porosity of SnO_2 nanospheres can effectively be tuned via precursor concentration, temperature and the removal of additive urea. High temperatures are shown to facilitate the dissolution of the nanospheres while elimination of additive urea removes any organic contaminant which reduces the effective surface area, thus rendering the structures to be more porous in nature. The operating temperature has a strong influence on the sensitivity of the sensor whereby a higher optimum operating temperature leads to a greater change in conductance and hence, greater sensitivity. In general, an increase in specific surface area of the sensor implies more surface sites for greater surface reactivity. The inner surfaces of the porous nanospheres are not fully utilized for gas detection due to the limitation of diffusion of the analyte gas. The sensing properties of nanospheres sensors are dependent on the gas reactivity on the surface as well as gas diffusivity through the sensing layers. The response and recovery times are found to correlate to the

reactivity rate of the analyte gas with the sensing material, which in turn depends on the operating temperature.

Acknowledgment

This work is supported by the National University of Singapore (NUS) grant R-263-000-532-112.

References

- [1] Z.X. Cai, X.Y. Li, X.Y. Zeng, Direct fabrication of SnO₂-based thick film gas sensor using Micropen direct writing and laser microcladding, *Sens. Actuator B* 137 (2009) 340–344.
- [2] W.Y. Yin, B.Q. Wei, C.W. Hu, In situ growth of SnO₂ nanowires on the surface of Au-coated Sn grains using water-assisted chemical vapor deposition, *Chem. Phys. Lett.* 471 (2009) 11–16.
- [3] Y. Shen, T. Yamazaki, Z. Liu, D. Meng, T. Kikuta, N. Nakatani, M. Saito, M. Mori, Microstructure and H₂ gas sensing properties of undoped and Pd-doped SnO₂ nanowires, *Sens. Actuator B* 135 (2009) 524–529.
- [4] C. Wang, X. Chu, M. Wu, Highly sensitive gas sensors based on hollow SnO₂ spheres prepared by carbon sphere template method, *Sens. Actuator B* 120 (2007) 508–513.
- [5] C. Nützenadal, A. Züttel, D. Chartouni, G. Schmid, L. Schlapbach, Critical size and surface effect of the hydrogen interaction of palladium clusters, *Eur. Phys. J.* 8 (2000) 245–250.
- [6] S. Kaciulis, G. Matogno, A. Galdikas, A. Mironas, A. Setkus, Influence of surface oxygen on chemoresistance of tin oxide film, *J. Vac. Sci. Technol. A* 14 (1996) 3164–3168.
- [7] F. Caruso, X. Shi, R.A. Caruso, A. Susha, Hollow titania spheres from layered precursor deposition on sacrificial colloidal core particles, *Adv. Mater.* 13 (2001) 740–744.
- [8] T. Liu, Y. Xie, B. Chu, Use of block copolymer micelles on formation of hollow MoO₃ nanospheres, *Langmuir* 16 (2000) 9015–9022.
- [9] X.W. Lou, C. Yuan, E. Rhoades, Q. Zhang, L.A. Archer, Encapsulation and Ostwald ripening of Au and Au–Cl complex nanostructures in silica shells, *Adv. Funct. Mater.* 16 (2006) 1679–1684.
- [10] L.M. Qi, J. Li, J.M. Ma, Biomimetic morphogenesis of calcium carbonate in mixed solutions of surfactants and double-hydrophilic block copolymers, *Adv. Mater.* 14 (2002) 300–303.
- [11] S.Y. Ho, A.S.W. Wong, G.W. Ho, Controllable porosity of monodispersed tin oxide nanospheres via an additive-free chemical route, *Cryst. Growth Des.* 9 (2009) 732–736.
- [12] R.L. Penn, J.F. Banfield, Imperfect oriented attachment: dislocation generation in defect-free nanocrystals, *Science* 281 (1998) 969–971.
- [13] M.E. Franke, T.J. Koplín, U. Simon, Metal and metal oxide nanoparticles in chemiresistors: Does the nanoscale matter? *Small* 2 (2006) 36–50.
- [14] G.J. Kim, X.H. Zhang, S. Kawi, Relationships between sensitivity, catalytic activity, and surface areas of SnO₂ gas sensors, *Sens. Actuator B* 60 (1999) 64–70.
- [15] Q. Zhao, Y. Gao, X. Bai, C. Wu, Y. Xie, Facile synthesis of SnO₂ hollow nanospheres and applications in gas sensors and electrocatalysts, *Eur. J. Inorg. Chem.* 8 (2006) 1643–1648.
- [16] G.J. Li, S. Kawi, Synthesis, characterization and sensing application of novel semiconductor oxides, *Talanta* 45 (1998) 759–766.
- [17] Y. Shimizu, A. Jono, T. Hyodom, M. Egashira, Preparation of large mesoporous SnO₂ powder for gas sensor application, *Sens. Actuator B* 108 (2005) 56–61.
- [18] Y. Shimizu, T. Maekawa, Y. Nakamura, M. Egashira, Effects of gas diffusivity and reactivity on sensing properties of thick film SnO₂-based sensors, *Sens. Actuator B* 46 (1998) 163–168.
- [19] M. Tiemann, Porous metal oxides as gas sensors, *Chem. Eur. J.* 13 (2007) 8376–8388.

Biographies

S.C. Yeow is currently a bachelor degree (honors) student from Electrical and Computer Engineering, National University of Singapore. His current research work is on the oxide mesoporous nanomaterials for hydrogen sensors applications.

W.L. Ong is currently a Ph.D. student of Electrical and Computer Engineering in National University of Singapore. He received his Bachelor (honors) degree in 2008 from Electrical and Computer Engineering, National University of Singapore. His current research work is on the oxide nanostructured materials for sensors and transistors applications.

A.S.W. Wong received his Ph.D. degree from the Department of Materials Science and Metallurgy at the University of Cambridge in 2006. His current research interests are thin film solar cell, sensors and electron microscopy.

G.W. Ho is an assistant professor of Electrical and Computer Engineering in National University of Singapore. She received her Ph.D. degree in Engineering from Nanoscience Centre, University of Cambridge in 2006, M.Sc. and B.Sc. from National University of Singapore in 2001. Her current research is focused on the study of the phenomena and manipulation of material at the nanoscale which revolves around the realization of solar cell, chemical sensor and energy harvesting systems.